Progress In Electromagnetics Research, Vol. 108, 433–447, 2010

EXTENDED DOUBLET BANDPASS FILTERS IMPLEMENTED WITH MICROSTRIP RESONATOR AND FULL-/HALF-MODE SUBSTRATE INTEGRATED CAVITIES

L.-S. Wu, J.-F. Mao, W. Shen, and W.-Y. Yin

Center for Microwave and RF Technologies
Shanghai Jiao Tong University
Shanghai 200240, China

Abstract—Two extended doublet bandpass filters with compact size and good spurious suppression characteristic are proposed. One is built up by a dual-mode microstrip resonator with a full-mode substrate integrated cavity, while the other is composed of a microstrip resonator and a half-mode cavity. The relationship between the location of their transmission zeros and the impedance ratio of the microstrip resonator is analyzed theoretically. Our proposed filters only occupy the areas of $0.69\lambda_0^2/\varepsilon_r$ and $0.51\lambda_0^2/\varepsilon_r$, and they also have wide upper stopband. The predicted performances are demonstrated by the reasonable agreement obtained between their simulated and measured S-parameters.

1. INTRODUCTION

The extended doublet topology has drawn much attention for filter design. Because two symmetric or asymmetric transmission zeros can be generated with a third-order building block, the extended doublet bandpass filters have some advantages, such as high frequency selectivity and miniaturized configuration [1]. In particular, the coupling scheme can be implemented easily with a dual-mode resonator and an additional single-mode resonator using planar microstrip structures [2, 3].

On the other hand, substrate integrated waveguides (SIWs) [4, 5] are attractive for the design of microwave and millimeter-wave circuits, due to their high Q-factor, high power handling capability, low cost,

Received 12 August 2010, Accepted 28 September 2010, Scheduled 1 October 2010
Corresponding author: L.-S. Wu (wallish@sjtu.edu.cn).

and easy integration with other planar circuits [6–12], etc.. Recently, some modifications, such as folded and half-mode SIWs [13–19], are presented to further reduce the size of SIW components.

The extended doublet filter has also been proposed using multilayer SIW cavity structures to make the component with the advantages of SIW [20]. To further reduce the size of extended doublet SIW filter, the authors proposed a bandpass filter using only one dual-mode SIW cavity with a complementary split ring resonator etched on its top metal plane [21], which is also an attempt for the hybrid realization of high-performance filter using both SIW and other planar resonators with more flexibility. However, the occupied area of the dual-mode cavity is still large and its spurious suppression characteristic is not good due to the impure mode spectrum of SIW structures.

In this article, two compact extended doublet bandpass filters are proposed using a dual-mode microstrip resonator and full-/half-mode SIW cavities. Since the SIW cavities are neither connected directly to the source nor the load nodes, the parasitic responses introduced by their higher-order resonant modes are not obvious. And the spurious suppression characteristics of the components are further improved by properly selecting the excitation structure. Our predicted filter performances have been demonstrated by the reasonable agreement obtained between the simulated and measured S-parameters.

2. ANALYSIS AND DESIGN

2.1. Dual-mode Microstrip Resonator

As shown in Figure 1, an extended doublet bandpass filter consists of three resonant nodes, where Nodes 1 and 2 can be replaced by the even and odd modes in a dual-mode resonator, and Node 3 can be formed using another resonator [2]. Because only two independent resonant structures are included, the whole geometry is compact, with loss and

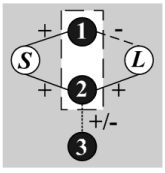

Figure 1. The coupling scheme of an extended doublet bandpass filter [2].

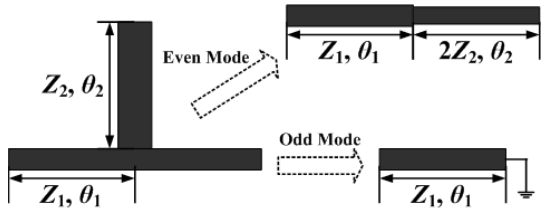

Figure 2. The configuration of the dual-mode microstrip resonator.

cost also reduced effectively.

In our design, the resonant behaviors of Nodes 1 and 2 are provided by a dual-mode microstrip resonator, as shown in Figure 2. The resonant frequency of the odd mode is controlled by the main body of the open-ended microstrip line, while that of the even mode is controlled by the open stub. If the two resonant frequencies are both equal to the designed central frequency f_0, both the electrical lengths θ_1 and θ_2 should be $\pi/2$ at the central frequency. The first higher-order mode is the second even mode, and its resonant frequency is about twice the central frequency.

2.2. Full-mode SIW Rectangular Cavity

Because almost no electromagnetic fields corresponding to the odd mode are distributed in the stub, the coupling between the microstrip resonator and another resonator (Node 3 in Figure 1) can only be achieved with the even mode of the dual-mode resonator. Thus, the even mode should play the role of Node 2 in our coupling scheme, while the odd mode corresponds to Node 1.

In order to make the filter with the advantages of SIWs, a full-mode SIW rectangular cavity is firstly utilized to implement Node 3. The structure shown in Figure 3 is applied, since the SIW cavity should only couple to the even mode of the microstrip resonator and the stub should be open-ended.

By this configuration, only the even resonant modes of the microstrip resonator and the SIW cavity can be coupled with each other. In other words, only the energies corresponding to the $TE_{2m-1,0,l}$-modes in the SIW cavity will be transmitted to the microstrip resonator, where both m and l are natural numbers. Thus, in order to suppress the spurious responses introduced by the higher-order modes of full-mode SIW cavity, we can make the resonant frequency f_{102} of its TE_{102}-mode equal to the resonant frequency f_{301} of its TE_{301}-mode. Since the differences between the physical

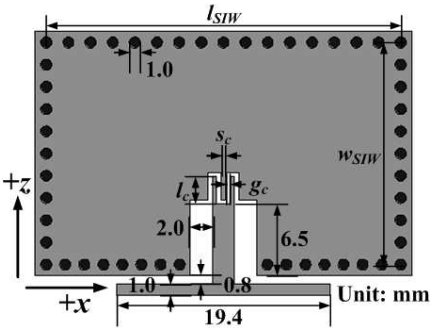

Figure 3. The structure of the dual-mode resonator and the full-mode SIW rectangular cavity which are coupled with each other.

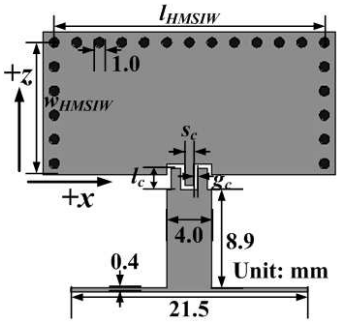

Figure 4. The structure of the dual-mode resonator and the half-mode SIW rectangular cavity which are coupled with each other.

and equivalent dimensions of the full-mode SIW cavity are small and negligible [22], we approximately have

$$\frac{c_0}{2\sqrt{\varepsilon_r}}\sqrt{\frac{1^2}{l_{SIW}^2}+\frac{2^2}{w_{SIW}^2}}=\frac{c_0}{2\sqrt{\varepsilon_r}}\sqrt{\frac{3^2}{l_{SIW}^2}+\frac{1^2}{w_{SIW}^2}} \tag{1}$$

where c_0 is the velocity of light in vacuum, ε_r is the relative permittivity of the substrate, l_{SIW} and w_{SIW} are the lengths of the sides vertical and parallel to $+z$ direction of the full-mode SIW cavity, respectively. From (1), we can obtain

$$\frac{w_{SIW}}{l_{SIW}}=\sqrt{\frac{3}{8}}\approx 0.61 \tag{2}$$

When (1) or (2) are satisfied, it is obtained that

$$l_{SIW} = \sqrt{\frac{11}{12}}\frac{c_0}{\sqrt{\varepsilon_r}f_0}\approx 0.96\frac{\lambda_0}{\sqrt{\varepsilon_r}} \tag{3}$$

$$\frac{f_{102}}{f_0} = \frac{f_{301}}{f_0}=\sqrt{\frac{35}{11}}\approx 1.78 \tag{4}$$

where the central frequency f_0 of the bandpass filter is equal to the resonant frequency f_{101} of the dominant mode in the full-mode SIW rectangular cavity. The initial values of its side lengths are determined by (3) and (2). Then, the full-mode SIW rectangular cavity occupies an area of about $0.56\lambda_0^2/\varepsilon_r$.

2.3. Half-mode SIW Cavity

In order to reduce the size of SIW cavity, half-mode technique is used. As shown in Figure 4, a rectangular half-mode substrate integrated cavity is coupled with the dual-mode microstrip resonator through its open side. To consider the length compensation of open side, the equivalent width of half-mode SIW cavity is approximated by [23]

$$w'_{HMSIW} \approx w_{HMSIW} + \left(0.05+\frac{0.30}{\varepsilon_r}\right)\ln\left(\frac{0.79w_{HMSIW}^2}{h^2}+\frac{104w_{HMSIW}-261}{h}+38+2.77h\right) \quad (5)$$

where both the units of w_{HMSIW} and h are mm.

The dominant even mode in half-mode SIW cavity is $TE_{1,0,0.5}$-mode, while the first two higher-order even modes are $TE_{1,0,1.5}$- and $TE_{3,0,0.5}$-modes. Then, their resonant frequencies $f_{1,0,1.5}$ and $f_{3,0,0.5}$ are set to the same value, i.e.,

$$\frac{c_0}{2\sqrt{\varepsilon_r}}\sqrt{\frac{1^2}{l_{HMSIW}^2}+\frac{1.5^2}{w'^2_{HMSIW}}} = \frac{c_0}{2\sqrt{\varepsilon_r}}\sqrt{\frac{3^2}{l_{HMSIW}^2}+\frac{0.5^2}{w'^2_{HMSIW}}} \quad (6)$$

So, we have

$$w'_{HMSIW} = \frac{1}{2}l_{HMSIW} = \frac{\sqrt{2}}{4}\frac{\lambda_0}{\sqrt{\varepsilon_r}} \quad (7)$$

$$\frac{f_{1,0,1.5}}{f_0} = \frac{f_{3,0,0.5}}{f_0} = \sqrt{5} \approx 2.24 \quad (8)$$

Thus, the half-mode SIW cavity only occupies about $0.25\lambda_0^2/\varepsilon_r$, 45% of the area of full-mode SIW rectangular cavity.

2.4. Coupling between SIW Cavity and Microstrip Resonator

When the microstrip resonator works in its even mode, the electric field reaches its maximum at the open end of stub and the magnetic field reaches its maximum at the 3-port conjunction. The electric field corresponding to the dominant mode of SIW resonator reaches the maximum at the middle of cavity, and the magnetic field reaches the maximum near the side wall. As shown in Figure 3, the electric coupling between the SIW cavity and the microstrip resonator is implemented using an interdigital structure. And the magnetic coupling between them is made negligible by adding a wide gap between the cavity and the microstrip open stub.

The electric coupling coefficients are controlled by the length l_c of fingers, the widths s_c and g_c of fingers and narrow gaps. In order to

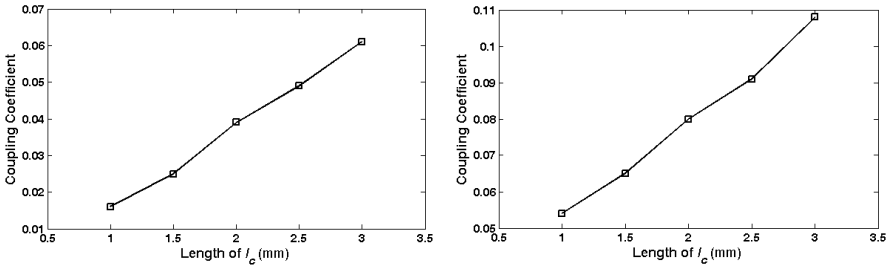

Figure 5. The coupling coefficient provided by the interdigital structure as functions of l_c for the (a) full- and (b) half-mode SIW cases.

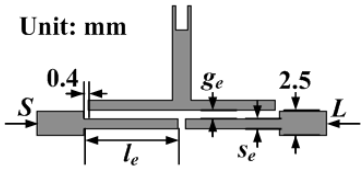

Figure 6. The external coupling structure used in our proposed filter.

reduce the influence of fabrication tolerance, the width g_c of gaps is set to 0.4 mm, and the width s_c of fingers on microstrip/SIW is set to 0.4 and 0.8 mm for the full- and half-mode SIW cases, respectively. Then, the coupling coefficients are extracted by [24]

$$k = \pm \frac{f_{p2}^2 - f_{p1}^2}{f_{p1}^2 + f_{p2}^2} \tag{9}$$

where f_{p1} and f_{p2} are the frequencies of two resonant peaks in simulations. The coupling coefficients are plotted in Figures 5(a) and (b) as functions of l_c for the two cases. The coupling coefficient in half-mode SIW case is larger than that in full-mode SIW case with the same value of l_c, mainly due to less normalized energy stored in the half-mode cavity than the full-mode one.

2.5. External Coupling

To excite the two resonant modes of microstrip resonator simultaneously, a pair of open-ended microstrip feedlines are used, whose length is close to half the length of microstrip resonator, as shown in Figure 6. The external coupling coefficients M_{S1} and M_{S2} can be tuned by changing the gap width g_e.

The normalized angular frequency of the transmission zeros provided by the extended doublet configuration is calculated by [2]

$$\Omega_z^2 = \frac{m_{23}^2}{1 - (m_{S2}/m_{S1})^2} \tag{10}$$

where m_{23} is the normalized electric coupling coefficient between Nodes 2 and 3, m_{S1} and m_{S2} are the normalized external coupling coefficients of Nodes 1 and 2, respectively. From (10), it is seen that the location of transmission zeros are determined by m_{S2}/m_{S1} and m_{23}.

m_{S1} and m_{S2} are expressed by [25]

$$m_{Si} = M_{Si}\sqrt{\frac{f_0}{BW}} \tag{11}$$

where i=1 and 2, and BW is the bandwidth of bandpass filter. So the ratio m_{S2}/m_{S1} is equal to M_{S2}/M_{S1}.

In general, the external coupling coefficient can be described by [24]

$$M_{Si} = \frac{1}{\sqrt{Q_{ei}}} = \sqrt{\frac{R_i}{2\pi f_0 L_i}} \tag{12}$$

where R_i is the external resistance looked from the i-th resonant node, Q_{ei} and L_i are the external quality factor and equivalent inductance of the i-th resonant node, respectively. Equation (12) can also be written as

$$M_{Si} = \sqrt{\frac{0.5I_{pi}^2 R_i}{2\pi f_0 \left(0.5I_{pi}^2 L_i\right)}} = \sqrt{\frac{P_i}{2\pi f_0 W_i}} \tag{13}$$

where I_{pi} is the equivalent peak current at the feed-point of the i-th resonant node, W_i and P_i are its corresponding stored energy and equivalent input (or output) power, respectively.

Then, we have

$$\frac{M_{S2}}{M_{S1}} = \frac{I_{p2}}{I_{p1}}\sqrt{\frac{W_1 R_2}{W_2 R_1}} \tag{14}$$

Because the two orthogonal resonant modes of the dual-mode microstrip resonator share the same excitation structure, their attached external resistance should be equal to each other, i.e.,

$$R_1 = R_2 \tag{15}$$

And their electromagnetic field distributions in the main body of microstrip resonator are very similar, so (15) can be further simplified

as

$$\frac{M_{S2}}{M_{S1}} = \sqrt{\frac{W_1'}{W_2'}} \tag{16}$$

where W_1' and W_2' are the stored energies of the two resonant modes when their equivalent peak currents I_{p1} and I_{p2} at the feed-point are equal to each other.

Set the maximum currents corresponding to the two resonant modes in the main body of microstrip resonator both to I_0. Then, the stored energy of odd mode is given by

$$W_1' = \int_{-\frac{l_1}{2}}^{\frac{l_1}{2}} \frac{1}{2} I_0^2 \frac{Z_1 \beta_1}{2\pi f_0} \cos^2(\beta_1 x)\, dx = \frac{I_0^2 Z_1}{8 f_0} \tag{17}$$

where β_1 is the phase constant of microstrip main body and l_1 is its length, which satisfy $\beta_1 l_1 = \pi$. And based on the continuity of current at the 3-port conjunction, the stored energy of even mode can be deduced as

$$\begin{aligned} W_2' \;=\; & 2\int_0^{\frac{l_1}{2}} \frac{1}{2} I_0^2 \frac{Z_1 \beta_1}{2\pi f_0} \cos^2(\beta_1 x)\, dx \\ & + \int_0^{l_2} \frac{1}{2} (2I_0)^2 \frac{Z_2 \beta_2}{2\pi f_0} \cos^2(\beta_2 x)\, dx = \frac{I_0^2 (Z_1 + 2Z_2)}{8 f_0} \end{aligned} \tag{18}$$

where β_2 is the phase constant of open stub and l_2 is the stub length, which satisfy $\beta_2 l_2 = \pi/2$. Thus, the ratio between two external coupling coefficients is obtained by

$$\frac{m_{S2}}{m_{S1}} = \sqrt{\frac{Z_1}{Z_1 + 2Z_2}} \tag{19}$$

And the transmission zeros are located at

$$\Omega_z = \pm\sqrt{1 + \frac{Z_1}{2Z_2}}\, |m_{23}| \tag{20}$$

From (20), it is concluded that the location of transmission zeros can easily be controlled by tuning the impedance ratio of two microstrip sections and the coupling coefficient between SIW cavity and microstrip resonator.

On the other hand, the first parasitic mode of microstrip resonator is the second even mode, and it resonates at about $2f_0$. In this case, the electrical lengths of both open-ended feedline and its corresponding coupled section of the microstrip resonator are about π, and they have the same normalized current (and voltage) distributions. Then, the magnetic and electric coupling coefficients between feedline and

resonator have opposite signs and similar values, which results in a weak total external coupling for the parasitic mode. Thus, its corresponding spurious response will be suppressed. This is similar to the discriminating coupling scheme between microstrip resonators [26].

3. RESULTS AND DISCUSSION

3.1. Full-mode SIW Case

A filter prototype with full-mode SIW cavity is designed with the central frequency of $f_0 = 5.0\,\text{GHz}$, the bandwidth of 0.2 GHz, the in-band ripple return loss of 15 dB, and two transmission zeros located at ± 1.5. Its coupling matrix is synthesized to be

$$M = \begin{array}{c} \\ S \\ 1 \\ 2 \\ 3 \\ L \end{array} \begin{array}{c} \begin{array}{ccccc} S & 1 & 2 & 3 & L \end{array} \\ \begin{bmatrix} 0 & 0.761 & 0.492 & 0 & 0 \\ 0.761 & 0 & 0 & 0 & -0.761 \\ 0.492 & 0 & 0 & -1.144 & 0.492 \\ 0 & 0 & -1.144 & 0 & 0 \\ 0 & -0.761 & 0.492 & 0 & 0 \end{bmatrix} \end{array} \tag{21}$$

where S and L mean the source and load nodes, respectively. According to (21), the ratio of characteristic impedances of two microstrip sections is calculated by

$$\frac{Z_2}{Z_1} = \frac{m_{S1}^2 - m_{S2}^2}{2m_{S2}^2} \approx 0.70 \tag{22}$$

The component was fabricated on a Taconic RF-30 substrate, with $\varepsilon_r = 3.0$, $\tan\delta = 0.0014$, and the thickness $h = 1.016\,\text{mm}$. Some geometrical parameters are $l_{SIW} = 32.3\,\text{mm}$, $w_{SIW} = 20.2\,\text{mm}$, $l_c = 2.5\,\text{mm}$, $s_c = 0.4\,\text{mm}$, $g_c = 0.4\,\text{mm}$, $l_e = 9.7\,\text{mm}$, $s_e = 1.0\,\text{mm}$, $g_e = 0.95\,\text{mm}$, and the other dimensions have been given in Figures 3 and 6. In this prototype, Z_1 and Z_2 are chosen to be 82.7 and 57.5 Ω, respectively.

The unloaded Q-factors of resonant nodes are obtained by

$$Q_1 = \frac{\beta_1}{2\alpha_1} \tag{23}$$

$$Q_2 = \left[\frac{Z_1}{Z_1 + 2Z_2}\frac{2\alpha_1}{\beta_1} + \frac{2Z_2}{Z_1 + 2Z_2}\frac{2\alpha_2}{\beta_2}\right]^{-1} \tag{24}$$

$$Q_3 = [\delta_c/h + \delta_c/l_{SIW} + \delta_c/w_{SIW} + \tan\delta]^{-1} \tag{25}$$

where δ_c is the skin depth of copper at f_0, α_1 and α_2 are the attenuation constants of two microstrip sections. Then, Q_1, Q_2 and Q_3 are

calculated to be 388, 406 and 418, respectively. The unloaded Q-factor of SIW cavity is a little larger than that of microstrip resonator. However, the SIW cavity has a large metal plane with good heat conductance, which is shorted by via arrays to the ground plane. Usually, the ground plane is connected with heat sink directly. So the SIW cavity helps to carry off heat source from the component and provides a good power handling capability for the whole component.

The photo of this fabricated prototype is shown in Figure 7(a), and the electric field distribution at its central frequency is shown in Figure 7(b). Its occupied area is $32.3 \times 25.7\,\text{mm}^2$, i.e., $0.69\lambda_0^2/\varepsilon_r$, while both the filters proposed in [20, 21] occupy $1.25\lambda_0^2/\varepsilon_r$. The measured S-parameters are plotted in Figure 8, with the simulated ones obtained by the full-wave EM simulator, Ansoft HFSS, also provided

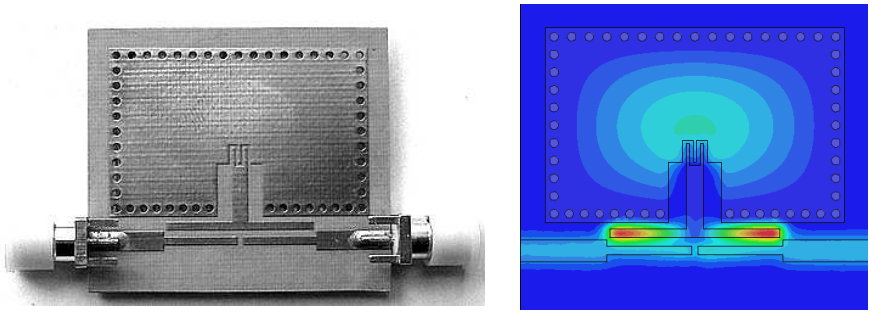

(a) (b)

Figure 7. The filter prototype with the full-mode SIW cavity: (a) its photo; and (b) the simulated electric field distribution at its central frequency.

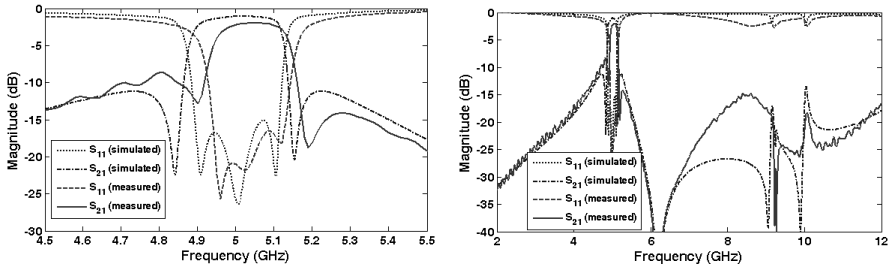

(a) (b)

Figure 8. Measured and simulated S-parameters of the prototype with the full-mode SIW cavity within (a) a narrow and (b) a wide frequency range.

for comparison. A reasonable agreement is obtained between them.

The measured central frequency is 5.04 GHz, 0.7% higher than the designed value, which is caused by the fabricated via diameter of 1.1 mm, larger than the designed value. The measured bandwidth is 0.16 GHz, 20% smaller than the simulated one. This is due to that the gaps between fingers are wider than their specified value and then the real coupling coefficient between SIW cavity and microstrip resonator is smaller than what we design. Since the bandwidth reduction will result in a larger insertion loss, the measured central insertion loss is 1.9 dB, 0.8 dB larger than the simulated one. The measured in-band return loss is better than 16.5 dB. Two transmission zeros are achieved at 4.90 and 5.19 GHz, which improve its frequency selectivity.

Since few parasitic resonant modes of the SIW cavity will disturb the filter performance and the second even mode of microstrip resonator cannot be excited in this topology, the proposed filter has a wide upper stopband under 15 dB, as shown in Figure 8(b). Both the filters reported in [20, 21] have two parasitic responses located around $0.63f_0$ and $1.26f_0$, while there is no spurious response below $2.4f_0$ for this filter. So it has a much better spurious suppression characteristic than its reported counterparts.

3.2. Half-mode SIW Case

The prototype for half-mode case is also designed with the central frequency of $f_0 = 5.0$ GHz. Its specified bandwidth is 0.3 GHz, the in-band ripple return loss is 20 dB, and two transmission zeros are produced at ± 2. Then, its corresponding coupling matrix is given by

$$M = \begin{array}{c} \\ S \\ 1 \\ 2 \\ 3 \\ L \end{array} \begin{array}{c} \begin{array}{ccccc} S & 1 & 2 & 3 & L \end{array} \\ \left[\begin{array}{ccccc} 0 & 0.785 & 0.615 & 0 & 0 \\ 0.785 & 0 & 0 & 0 & -0.785 \\ 0.615 & 0 & 0 & -1.242 & 0.615 \\ 0 & 0 & -1.242 & 0 & 0 \\ 0 & -0.785 & 0.615 & 0 & 0 \end{array}\right] \end{array} \tag{26}$$

The photo of fabricated filter is shown in Figure 9(a), with the electric field at its central frequency also plotted in Figure 9(b). Its simulated and measured S-parameters are plotted in Figure 10. The critical geometrical parameters are optimized to be $l_{HMSIW} = 24.5$ mm, $w_{HMSIW} = 12.0$ mm, $l_c = 2.0$ mm, $s_c = 0.8$ mm, $g_c = 0.4$ mm, $l_e = 9.7$ mm, $s_e = 0.4$ mm, and $g_e = 1.1$ mm. The other parameters have been given in Figures 4 and 6. And Z_1 is chosen to be 118 Ω while Z_2 is 37 Ω. Note that the ratio of Z_2 to Z_1 here is much smaller than that in the previous case.

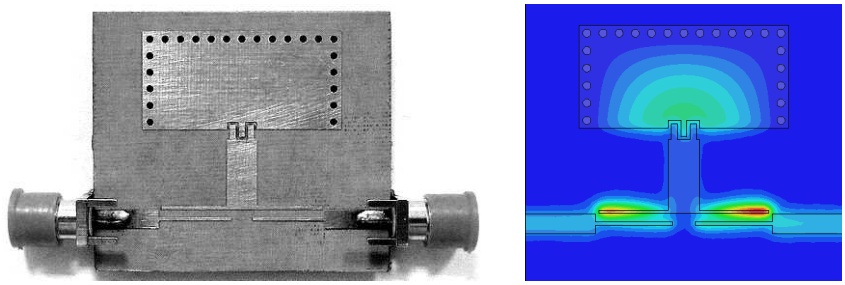

(a) (b)

Figure 9. The filter prototype with the half-mode SIW cavity: (a) its photo; and (b) the simulated electric field distribution at its central frequency.

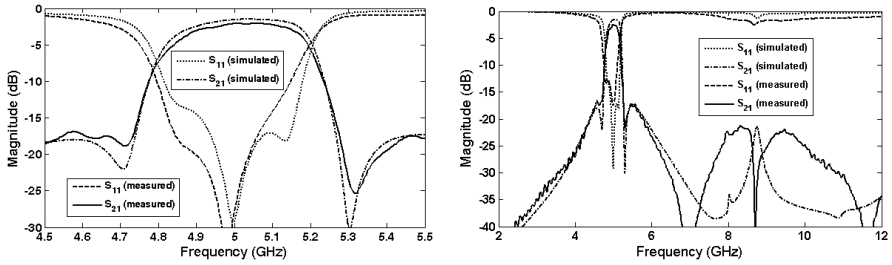

(a) (b)

Figure 10. Measured and simulated S-parameters of the prototype with the half-mode SIW cavity within (a) a narrow and (b) a wide frequency range.

Q_1 and Q_2 are calculated to be 319 and 356 by (23) and (24) in the half-mode SIW case, respectively. As an expansion of (25), the unloaded Q-factor of half-mode SIW cavity can be estimated by

$$Q_3 = \left[\delta_c/h + \delta_c/l_{HMSIW} + \delta_c/(2w_{HMSIW}) + \tan\delta + Q_r^{-1}\right]^{-1} \quad (27)$$

where Q_r is the Q-factor due to its radiation loss, since an additional open side is introduced in this case. However, no closed-from equation has been reported for the prediction of Q_r till now. By full-wave simulation, Q_3 is exacted to be about 400, 10–20% better than that of microstrip resonator.

The filter size is $25.2 \times 24.5\,\text{mm}^2$, about $0.51\lambda_0^2/\varepsilon_r$. Its measured central frequency and bandwidth are 4.99 and 0.26 GHz, respectively. The measured insertion loss is 2.1 dB at the central frequency, and the measured in-band return loss is better than 13 dB. There are two transmission zeros located at 4.71 and 5.32 GHz, as predicted. Since the mode spectrum of half-mode SIW cavity is purer than that of full-

mode SIW cavity, the former has a better upper stopband under 20 dB, as shown in Figure 10(b). It is observed that the measured transmission coefficient in the upper stopband is different from the simulated one, which is mainly caused by some weak parasitic coupling sensitive to fabrication tolerance.

4. CONCLUSION

Two compact extended doublet bandpass filters are proposed using a dual-mode microstrip resonator and full-/half-mode SIW rectangular cavities. In order to present the physical mechanism of the extended doublet topology, the relationship between the location of its symmetric transmission zeros and the impedance ratio of microstrip resonator is analyzed theoretically. The sizes of our proposed filters are reduced by about 45% and 59%, when compared with their previously reported extended doublet SIW counterparts. By our proposed coupling structure, the parasitic responses introduced by the higher-order resonant modes of SIW cavities are not obvious. And the spurious suppression characteristic can be further improved by the properly selected excitation structure. Our predicted performances have been demonstrated by the reasonable agreement obtained between the simulated and measured S-parameters of two filter prototypes.

ACKNOWLEDGMENT

This work was supported by the National Natural Science Foundation of China under Grant 60821062, by the National Natural Science Foundation of China under Grant 61001014, by the National Basic Research Program of China under Grant 2009CB320204, and by Taconic Advanced Material Company Ltd., Suzhou, China.

REFERENCES

1. Amari, S. and U. Rosenberg, "New building blocks for modular design of elliptic and self-equalized filters," *IEEE Trans. Microw. Theory Tech.*, Vol. 52, No. 2, 721–736, Feb. 2004.
2. Liao, C.-K., P.-L. Chi, and C.-Y. Chang, "Microstrip realization of generalized Chebyshev filters with box-like coupling schemes," *IEEE Trans. Microw. Theory Tech.*, Vol. 55, No. 1, 147–153, Jan. 2007.
3. Zhou, M.-Q., X.-H. Tang, and F. Xiao, "Miniature microstrip bandpass filter using resonator-embedded dual-mode resonator

based on source-load coupling," *IEEE Microw. Wireless Compon. Lett.*, Vol. 20, No. 3, 139–141, Mar. 2010.

4. Piloto, A., K. Leahy, B. Flanick, and K. A. Zaki, "Waveguide filters having a layered dielectric structures," U.S. Patent 5382931, Jan. 17, 1995.
5. Uchimura, H., T. Takenoshita, and M. Fujii, "Development of a laminated waveguide," *IEEE Trans. Microw. Theory Tech.*, Vol. 46, No. 12, 2438–2443, Dec. 1998.
6. Deslandes, D. and K. Wu, "Integrated microstrip and rectangular waveguide in planar form," *IEEE Microw. Wireless Compon. Lett.*, Vol. 11, No. 2, 68–70, Feb. 2001.
7. Ismail, A., M. S. Razalli, M. A. Mahdi, R. S. A. Raja Abdullah, N. K. Noordin, and M. F. A. Rasid, "X-band trisection substrate-integrated waveguide quasi-elliptic filter," *Progress In Electromagnetics Research*, Vol. 85, 133–145, 2008.
8. Hammou, D., E. Moldovan, and S. O. Tatu, "V-band microstrip to standard rectangular waveguide transition using a substrate integrated waveguide (SIW)," *Journal of Electromagnetic Waves and Applications*, Vol. 23, No. 2–3, 221–230, 2009.
9. Lin, S., S. Yang, A. E. Fathy, and A. Elsherbini, "Development of a novel UWB Vivaldi antenna array using SIW technology," *Progress In Electromagnetics Research*, Vol. 90, 369–384, 2009.
10. Souzangar, P. and M. Shahabadi, "Numerical multimode thru-line (TL) calibration technique for substrate integrated waveguide circuits," *Journal of Electromagnetic Waves and Applications*, Vol. 23, No. 13, 1785–1793, 2009.
11. Tao, Y. and Z. Shen, "Broadband substrate integrated waveguide orthomode transducers," *Journal of Electromagnetic Waves and Applications*, Vol. 23, No. 16, 2099–2108, 2009.
12. Li, R., X. Tang, and F. Xiao, "A novel substrate integrated waveguide square cavity dual-mode filter," *Journal of Electromagnetic Waves and Applications*, Vol. 23, No. 17–18, 2523–2529, 2009.
13. Grigoropoulos, N., B. S. Izquierdo, and P. R. Young, "Substrate integrated folded waveguides (SIFW) and filters," *IEEE Microw. Wireless Compon. Lett.*, Vol. 15, No. 12, 829–831, Dec. 2005.
14. Wang, R., L.-S. Wu, and X.-L. Zhou, "Compact folded substrate integrated waveguide cavities and bandpass filter," *Progress In Electromagnetics Research*, Vol. 84, 135–147, 2008.
15. Wang, Y.-Q., W. Hong, Y.-D. Dong, B. Liu, H.-J. Tang, J.-X. Chen, X.-X. Yin, and K. Wu, "Half mode substrate integrated waveguide (HMSIW) bandpass filter," *IEEE Microw. Wireless*

Compon. Lett., Vol. 17, No. 4, 265–267, Apr. 2007.

16. Wu, L.-S., X.-L. Zhou, W.-Y. Yin, C.-T. Liu, L. Zhou, J.-F. Mao, and H.-L. Peng, "A new type of periodically loaded half-mode substrate integrated waveguide and its applications," *IEEE Trans. Microw. Theory Tech.*, Vol. 58, No. 4, 882–893, Apr. 2010.
17. Wang, Z.-G., X.-Q. Li, S.-P. Zhou, B. Yan, R.-M. Xu, and W.-G. Lin, "Half mode substrate integrated folded waveguide (HMSIFW) and partial H-plane bandpass filter," *Progress In Electromagnetics Research*, Vol. 101, 203–216, 2010.
18. Hwang, R.-B. and C.-Y. Chin, "Substrate integrated waveguides with moats," *Journal of Electromagnetic Waves and Applications*, Vol. 23, No. 8–9, 1101–1112, 2009.
19. Song, Q., H. R. Cheng, X. H. Wang, L. Xu, X.-Q. Chen, and X.-W. Shi, "Novel wideband bandpass filter integrating HMSIW with DGS," *Journal of Electromagnetic Waves and Applications*, Vol. 23, No. 14–15, 2031–2040, 2009.
20. Wei, Q.-F., Z.-F. Li, and H.-G. Shen, "Dual-mode filters based on substrate integrated waveguide by multilayer LTCC technology," *Microw. Opt. Technol. Lett.*, Vol. 50, No. 11, 2788–2790, Nov. 2008.
21. Wu, L.-S., X.-L. Zhou, Q.-F. Wei, and W.-Y. Yin, "An extended doublet substrate integrated waveguide (SIW) bandpass filter with a complementary split ring resonator (CSRR)," *IEEE Microw. Wireless Compon. Lett.*, Vol. 19, No. 12, 777–779, Dec. 2009.
22. Yan, L., W. Hong, G. Hua, J.-X. Chen, K. Wu, and T.-J. Cui, "Simulation and experiment on SIW slot array antennas," *IEEE Microw. Wireless Compon. Lett.*, Vol. 14, No. 9, 446–448, Sep. 2004.
23. Lai, Q.-H., C. Fumeaux, W. Hong, and R. Vahldieck, "Characterization of the propagation properties of the half-mode substrate integrated waveguide," *IEEE Trans. Microw. Theory Tech.*, Vol. 57, No. 8, 1996–2004, Aug. 2009.
24. Hong, J.-S. and M. J. Lancaster, *Microstrip Filters for RF/Microwave Applications*, Wiley, New York, 2001.
25. Macchiarella, G., "Generalized coupling coefficient for filters with nonresonant nodes," *IEEE Microw. Wireless Compon. Lett.*, Vol. 18, No. 12, 773–775, Dec. 2008.
26. Zhang, X.-Y. and Q. Xue, "Harmonic-suppressed bandpass filter based on discriminating coupling," *IEEE Microw. Wireless Compon. Lett.*, Vol. 19, No. 11, 695–697, Nov. 2009.